Mechanics of self-folding of single-layer graphene

IOP PUBLISHING JOURNAL OF PHYSICS D: APPLIED PHYSICS

J. Phys. D: Appl. Phys. **46** (2013) 055308 (6pp) doi:10.1088/0022-3727/46/5/055308

Mechanics of self-folding of single-layer graphene

Xianhong Meng[1], Ming Li[2,4], Zhan Kang[2], Xiaopeng Zhang[2] and Jianliang Xiao[3,4]

[1] School of Aeronautic Science and Engineering, Beihang University, Beijing 100191, People's Republic of China

[2] State Key Laboratory of Structural Analysis for Industrial Equipment, Dalian University of Technology, Dalian 116024, People's Republic of China

[3] Department of Mechanical Engineering, University of Colorado, Boulder, CO 80309-0427, USA

E-mail: mingli@dlut.edu.cn and Jianliang.Xiao@colorado.edu

Received 16 October 2012, in final form 30 November 2012
Published 8 January 2013
Online at stacks.iop.org/JPhysD/46/055308

Abstract

The extreme out-of-plane flexibility makes single-layer graphene vulnerable to self-folding, driven by van der Waals interactions. Racket shaped bilayer graphene edges form after self-folding, which can significantly affect the electrical properties of graphenes. To study the self-folding behaviour, a theoretical model based on finite deformation beam theory is established. The critical folding lengths for both metastable and stable self-folding, as well as the edge profile of a folded single-layer graphene, are given. They all agree very well with MD simulations. MD simulations also show that folding directions do not have strong influence on the shape of folded graphene edges.

(Some figures may appear in colour only in the online journal)

1. Introduction

Single-layer graphenes, formed by one layer of hexagonally patterned carbon atoms, possess unique electronic and mechanical properties [1–7], and have many potential applications, such as graphene electronics, gas separation and nanoelectromechanical systems (NEMS) [8–13]. In addition to free standing single-layer graphene, a novel nanostructure of graphene was discovered, with two graphene layers connected by a continuous curved edge, i.e. graphene bilayer edge [14–16]. The curved edge resembles the structure of a single-wall carbon nanotube, and can have strong influence on the electronic and magnetic properties of graphenes [17–20]. Graphene bilayer edges can be formed by scratching, high temperature annealing or back folding by electron beam induced sputtering [21, 22]. Very recently, Zhang *et al* reported that random mechanical stimulation can also induce formation of graphene bilayer edges via self-folding of single-layer graphenes dispersed in solution [14]. In this process, the van der Waals interaction acts as the main driving force for the self-folding, due to the exceptionally low bending stiffness of single-layer graphenes, while mechanical stimulation only helps initiate self-folding and overcome energy barriers. Study of the self-folding mechanics for single-layer graphenes can reveal the folding behaviour, and therefore may have important implications for their application in nanoelectronics and nanotechnology.

Similar self-folding and self-collapse behaviours have also been observed in carbon nanotubes [23–26]. Theoretical studies have revealed the critical length for nanotube self-folding [23–24]. Very recently, Cranford *et al* also studied the folding of graphene sheets [27]. However, the small deformation models presented in these studies cannot accurately predict the shape of a graphene bilayer edge, which could be important for studying the electronic and magnetic properties.

In this paper, an analytical model based on finite deformation beam theory [28] is developed to study the self-folding of single-layer graphene, which can accurately predict the critical length of graphene for self-folding and the shape of the folded edge. Molecular dynamics (MD) simulations were carried out to verify the analytical model. It is also

[4] Authors to whom any correspondence should be addressed.

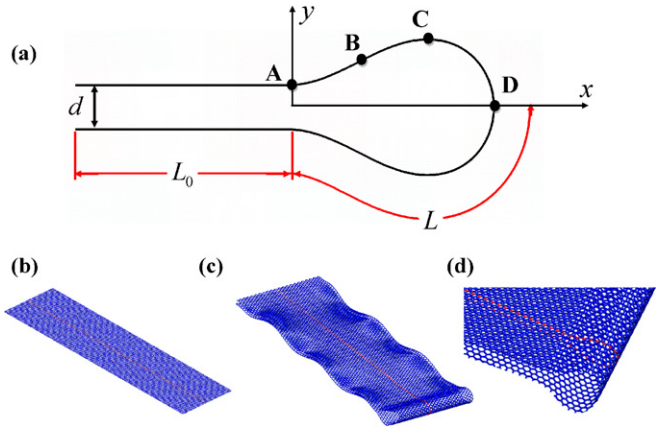

Figure 1. (*a*) Schematic illustration of a folded single-layer graphene. The flat (*b*) and the folded (*c*) states of a single-layer graphene obtained from MD simulations. A magnified view of the folded graphene edge is shown in (*d*).

demonstrated by MD simulations that the folding direction (or the chirality of folded edge) does not show a significant effect on the shape of the folded graphene edge.

2. Theoretical model

Figure 1(*a*) shows the schematic diagram of a folded single-layer graphene, which consists of a curved region of length $2L$ and a flat region of length L_0. The graphene adheres within the flat region due to van der Waals interaction, and the interlayer distance between the parallel, adhered region of the folded graphene is d. The curved region is due to the resistance to bending of the graphene, which can be characterized by the bending stiffness EI. The total length of the folded graphene is $L_{\text{tot}} = 2(L + L_0)$.

The self-folding phenomenon results from competition between the adhesion energy due to van der Waals interaction U_{adhesion} over the flat region and the bending energy U_{bend} over the curved region. The van der Waals interaction tends to fold the graphene and maximize the flat region, while the bending energy resists this trend and tends to unfold the graphene. We define the flat graphene before folding as the ground state, then the energy of the folded graphene is $U_{\text{tot}} = U_{\text{bend}} + U_{\text{adhesion}}$, where the bending energy U_{bend} will be obtained later, the adhesion energy $U_{\text{adhesion}} = -\gamma L_0$, and γ is the binding energy per unit area of graphene. If the graphene is very long, the adhesion energy exceeds the bending energy, i.e. $U_{\text{tot}} < 0$, the self-folded graphene is energetically favourable. If the graphene is very short, the adhesion energy is too small to support the bending, i.e. $U_{\text{tot}} > 0$, the flat graphene is more stable. Therefore, there exists a critical length $L^{\text{c}}_{\text{tot}}$, above which graphene self-folding occurs.

The graphene can be modelled as a beam with bending stiffness EI. Due to symmetry, only the top half of the graphene is analysed. The equilibrium equations of a beam are given as

$$\frac{\mathrm{d}M}{\mathrm{d}s} + V = 0, \qquad \frac{\mathrm{d}V}{\mathrm{d}s} + N\frac{\mathrm{d}\theta}{\mathrm{d}s} = 0, \qquad \frac{\mathrm{d}N}{\mathrm{d}s} - V\frac{\mathrm{d}\theta}{\mathrm{d}s} = 0, \tag{1}$$

where θ is the rotation angle, s is the arc length measured from point A, M, V and N are the bending moment, shear force and normal force within the beam, respectively. The curved top half of the graphene can be divided into three parts by four points, A, B, C and D, as shown in figure 1(*a*) A and D are the left most and right most points in the curved region of the graphene, with curvature κ_0 and rotation angle $\theta = 0$ at A, and curvature $-\kappa_1$ and rotation angle $\theta = -\pi/2$ at D. C is the top most point of the curved region, with curvature $-\kappa_0$ and rotation angle $\theta = 0$ (this can be proven later by equation (9)). B is a point between A and C, with 0 curvature. The Cartesian coordinate system is defined such that the x-axis is along the symmetric axis, and the y-axis passes through A, as shown in figure 1(*a*). The boundary conditions are given as

$$\begin{aligned} y &= \frac{d}{2}, \quad \theta = 0 && \text{at A,} \\ y &= 0, \quad \theta = -\frac{\pi}{2} && \text{at D.} \end{aligned} \tag{2}$$

Since $M = \mathrm{EI}(\mathrm{d}\theta/\mathrm{d}s) = \mathrm{EI}\kappa$, eliminating shear force V in equation (1) gives the equilibrium equations to be

$$-\mathrm{EI}\frac{\mathrm{d}^2}{\mathrm{d}s^2}\left(\frac{\mathrm{d}\theta}{\mathrm{d}s}\right) + N\frac{\mathrm{d}\theta}{\mathrm{d}s} = 0, \qquad \frac{\mathrm{d}N}{\mathrm{d}s} + \mathrm{EI}\frac{\mathrm{d}}{\mathrm{d}s}\left(\frac{\mathrm{d}\theta}{\mathrm{d}s}\right)\cdot\frac{\mathrm{d}\theta}{\mathrm{d}s} = 0. \tag{3}$$

Integrating the 2nd equation in equation (3) with respect to s gives the normal force inside the graphene as

$$N = -\frac{\mathrm{EI}}{2}\left(\frac{\mathrm{d}\theta}{\mathrm{d}s}\right)^2 + N_0, \tag{4}$$

where N_0 is an integral constant to be determined later. Substituting equation (4) into the 1st equation in equation (3) and integration yields

$$\frac{\mathrm{d}\kappa}{\mathrm{d}s} = -\sqrt{\frac{\kappa_1^4 - \kappa^4}{4} - \frac{N_0}{\mathrm{EI}}(\kappa_1^2 - \kappa^2)}, \tag{5}$$

where the conditions $\mathrm{d}\kappa/\mathrm{d}s = 0$ at D due to symmetry and $\mathrm{d}\kappa/\mathrm{d}s < 0$ from A to D are used.

Using the inverse of equation (5), integrating from A to D gives the half-length of the curved region to be

$$L = \int_{-\kappa_1}^{\kappa_0} \frac{\mathrm{d}\kappa}{\sqrt{\frac{\kappa_1^4-\kappa^4}{4} - \frac{N_0}{\mathrm{EI}}(\kappa_1^2 - \kappa^2)}}. \tag{6}$$

Using $\mathrm{d}y = \mathrm{d}s \cdot \sin\theta$ and equation (5), the vertical coordinate can be obtained as

$$y = \frac{d}{2} + \int_{\kappa_0}^{\kappa} \frac{-\sin\theta\,\mathrm{d}\kappa}{\sqrt{\frac{\kappa_1^4-\kappa^4}{4} - \frac{N_0}{\mathrm{EI}}(\kappa_1^2 - \kappa^2)}}. \tag{7}$$

Applying the boundary condition $y = 0$ at D from equation (2) in equation (7) gives

$$-\frac{d}{2} = \int_{\kappa_0}^{-\kappa_1} \frac{-\sin\theta\,\mathrm{d}\kappa}{\sqrt{\frac{\kappa_1^4-\kappa^4}{4} - \frac{N_0}{\mathrm{EI}}(\kappa_1^2 - \kappa^2)}}. \tag{8}$$

Substituting $\kappa = \mathrm{d}\theta/\mathrm{d}s$ into equation (5) and integration yields the rotation angle θ expressed in terms of the curvature κ as

$$\theta = -\sin^{-1}\frac{\kappa^2/2 - N_0/\mathrm{EI}}{\kappa_1^2/2 - N_0/\mathrm{EI}} + \sin^{-1}\frac{\kappa_0^2/2 - N_0/\mathrm{EI}}{\kappa_1^2/2 - N_0/\mathrm{EI}}. \quad (9)$$

Applying the boundary condition $\theta = -\pi/2$ at D from equation (2) in equation (9) gives

$$N_0 = \frac{\mathrm{EI}}{2}\kappa_0^2. \quad (10)$$

Then equation (9) can be simplified as

$$\theta = -\sin^{-1}\frac{\kappa^2 - \kappa_0^2}{\kappa_1^2 - \kappa_0^2}, \qquad \text{or}$$
$$\kappa = \begin{cases} \sqrt{\kappa_0^2 - (\kappa_1^2 - \kappa_0^2)\sin\theta}, & \text{between A, B,} \\ -\sqrt{\kappa_0^2 - (\kappa_1^2 - \kappa_0^2)\sin\theta}, & \text{between B, D.} \end{cases} \quad (11)$$

Use equations (10) and (11), equations (6) and (8) can be expressed as

$$L = \int_0^{\frac{\pi}{2}} \frac{\mathrm{d}\theta}{\sqrt{\kappa_0^2 + \sin\theta(\kappa_1^2 - \kappa_0^2)}} + 2\int_0^{\sin^{-1}\frac{\kappa_0^2}{\kappa_1^2-\kappa_0^2}} \frac{\mathrm{d}\theta}{\sqrt{\kappa_0^2 - \sin\theta(\kappa_1^2 - \kappa_0^2)}} \quad (12)$$

and

$$\frac{d}{2} = -2\int_0^{\sin^{-1}\frac{\kappa_0^2}{\kappa_1^2-\kappa_0^2}} \frac{\sin\theta\,\mathrm{d}\theta}{\sqrt{\kappa_0^2 - (\kappa_1^2 - \kappa_0^2)\sin\theta}} + \int_0^{\frac{\pi}{2}} \frac{\sin\theta\,\mathrm{d}\theta}{\sqrt{\kappa_0^2 + (\kappa_1^2 - \kappa_0^2)\sin\theta}}. \quad (13)$$

From equations (12) and (13), the two unknown curvatures κ_0 and κ_1 can be obtained in terms of the half length of curved region L and the interlayer distance d.

Using $\mathrm{d}x = \mathrm{d}s \cdot \cos\theta$, equations (5) and (7), the Cartesian coordinates of any point in the curved region of graphene can be obtained as

$$x = \begin{cases} \displaystyle\int_0^{\theta} \frac{\cos\theta\,\mathrm{d}\theta}{\sqrt{\kappa_0^2 - (\kappa_1^2 - \kappa_0^2)\sin\theta}}, & \text{in AB,} \\ \displaystyle\int_0^{\sin^{-1}\frac{\kappa_0^2}{\kappa_1^2-\kappa_0^2}} \frac{\cos\theta\,\mathrm{d}\theta}{\sqrt{\kappa_0^2 - (\kappa_1^2 - \kappa_0^2)\sin\theta}} + \int_{\theta}^{\sin^{-1}\frac{\kappa_0^2}{\kappa_1^2-\kappa_0^2}} \frac{\cos\theta\,\mathrm{d}\theta}{\sqrt{\kappa_0^2 - (\kappa_1^2 - \kappa_0^2)\sin\theta}}, & \text{in BC,} \\ \displaystyle 2\int_0^{\sin^{-1}\frac{\kappa_0^2}{\kappa_1^2-\kappa_0^2}} \frac{\cos\theta\,\mathrm{d}\theta}{\sqrt{\kappa_0^2 - (\kappa_1^2 - \kappa_0^2)\sin\theta}} - \int_0^{\theta} \frac{\cos\theta\,\mathrm{d}\theta}{\sqrt{\kappa_0^2 - (\kappa_1^2 - \kappa_0^2)\sin\theta}}, & \text{in CD,} \end{cases}$$

$$y = \begin{cases} \displaystyle\frac{d}{2} + \int_0^{\theta} \frac{\sin\theta\,\mathrm{d}\theta}{\sqrt{\kappa_0^2 - (\kappa_1^2 - \kappa_0^2)\sin\theta}}, & \text{in AB,} \\ \displaystyle\frac{d}{2} + \int_0^{\sin^{-1}\frac{\kappa_0^2}{\kappa_1^2-\kappa_0^2}} \frac{\sin\theta\,\mathrm{d}\theta}{\sqrt{\kappa_0^2 - (\kappa_1^2 - \kappa_0^2)\sin\theta}} + \int_{\theta}^{\sin^{-1}\frac{\kappa_0^2}{\kappa_1^2-\kappa_0^2}} \frac{\sin\theta\,\mathrm{d}\theta}{\sqrt{\kappa_0^2 - (\kappa_1^2 - \kappa_0^2)\sin\theta}}, & \text{in BC,} \\ \displaystyle\frac{d}{2} + 2\int_0^{\sin^{-1}\frac{\kappa_0^2}{\kappa_1^2-\kappa_0^2}} \frac{\sin\theta\,\mathrm{d}\theta}{\sqrt{\kappa_0^2 - (\kappa_1^2 - \kappa_0^2)\sin\theta}} - \int_0^{\theta} \frac{\sin\theta\,\mathrm{d}\theta}{\sqrt{\kappa_0^2 - (\kappa_1^2 - \kappa_0^2)\sin\theta}}, & \text{in CD.} \end{cases} \quad (14)$$

The bending energy of the curved region of the graphene U_{bend} can be obtained as

$$U_{\mathrm{bend}} = 2\int_0^L \frac{\mathrm{EI}}{2}\kappa^2\,\mathrm{d}s = \mathrm{EI}\left[2\int_0^{\sin^{-1}\frac{\kappa_0^2}{\kappa_1^2-\kappa_0^2}} \sqrt{\kappa_0^2 - (\kappa_1^2 - \kappa_0^2)\sin\theta}\,\mathrm{d}\theta + \int_0^{\frac{\pi}{2}} \sqrt{\kappa_0^2 + (\kappa_1^2 - \kappa_0^2)\sin\theta}\,\mathrm{d}\theta\right]. \quad (15)$$

The total energy of the folded graphene is

$$U_{\mathrm{tot}} = U_{\mathrm{bend}} - \frac{\gamma}{2}(L_{\mathrm{tot}} - 2L). \quad (16)$$

For any given interlayer distance d, the total energy of the folded graphene is a sole function of the half-length of curved region L, and therefore minimization of the total energy U_{tot} with respect to L gives the solution to the graphene self-folding. Numerical methods will be used to solve equation (16).

3. MD simulation

MD simulations have been performed to investigate the self-folding of graphene. The large-scale molecular simulations package LAMMPS [29] and visualization program VMD [30] were employed to run and analyse the simulations. The C–C atomic interactions in graphene are characterized by the adaptive intermolecular reactive empirical bond order (AIREBO) potential [31], which consists of the reactive empirical bond order (REBO) term [32] characterizing the short-range C–C bonding and the Lennard-Jones term describing the long-range van der Waals interaction. Therefore, the total potential energy of a graphene is obtained as

$$E = \frac{1}{2}\sum_i \sum_{j\neq i} [E_{ij}^{\mathrm{REBO}} + E_{ij}^{\mathrm{LJ}}]. \quad (17)$$

The REBO term $E_{ij}^{\mathrm{REBO}} = V^{\mathrm{R}}(r_{ij}) + b_{ij}V^{\mathrm{A}}(r_{ij})$, where r_{ij} is the distance between two atoms, b_{ij} represents the bond order function, and $V^{\mathrm{R}}(r_{ij})$ and $V^{\mathrm{A}}(r_{ij})$ are repulsive and attractive terms, respectively [32]. The van der Waals interaction is

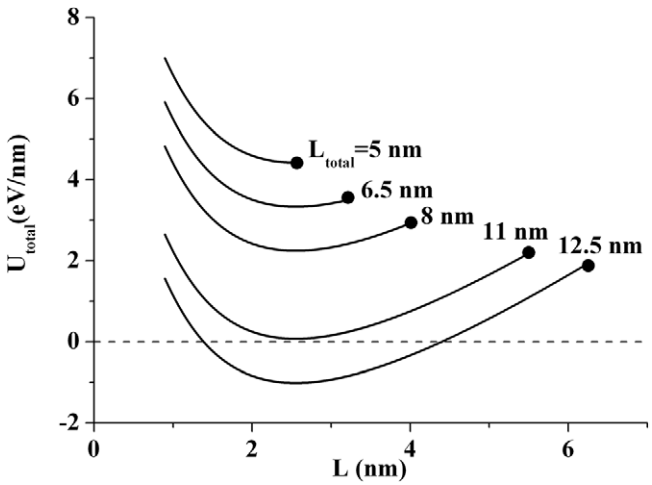

Figure 2. The total system energy of a folded single-layer graphene U_{tot} given by equation (16) versus the half length of the folded region L, for different total graphene length L_{tot}. The dots mean the curved region half length L reaches $L_{\text{tot}}/2$.

modelled by Lennard-Jones potential, $E_{ij}^{\text{LJ}} = 4\varepsilon[(\sigma/r_{ij})^{12} - (\sigma/r_{ij})^{6}]$, with $\varepsilon = 2.4$ meV, and $\sigma = 0.34$ nm [26]. The cut-off distance for van der Waals interaction is set to be 10.5 Å.

In the MD simulations, rectangular graphene sheets of length 40 nm and width 10 nm, as shown in figure 1(*b*), were adopted. The length was sufficiently large to ensure stable self-folding. A constant temperature of 0 K was ensured during the simulation to eliminate the atomic vibration and to compare with theoretical modelling. To facilitate the self-folding during simulation, the two ends of the flat graphene sheet were brought together by externally applied loading. Subsequent removal of the external loading and relaxation of the system lead to self-folding of the graphene, induced by van der Waals interactions among carbon atoms. The final configuration of a folded graphene sheet is shown in figure 1(*c*). Figure 1(*d*) shows a magnified view of the folded graphene edge near the symmetric plane marked by red line, which resembles a racket shape. Graphene sheets of different lengths are also used in MD simulations, to identify the critical length for metastable and stable self-folding.

4. Results and discussion

For analytical modelling, the bending stiffness, interlayer spacing and adhesion energy per unit area of the single-layer graphene obtained by first principle calculations and atomistic simulations are adopted, with EI $= 1.4$ eV, $d = 0.34$ nm and $\gamma = 1.45\,\text{eV nm}^{-2}$ [33–37]. Then the total system energy given by equation (16) can be plotted versus the half length L of the curved region, for different total graphene lengths, as shown in figure 2. The dots mean the curved region half length L reaches $L_{\text{tot}}/2$. It shows that the curved region reaches optimal state when $L = 2.5$ nm, and the two curvature values of κ_0 and κ_1 are obtained as 1.02 and 1.915, respectively. As the total length of the graphene L_{tot} increases, the total system energy U_{tot} decreases. Then the critical total length for stable self-folding is also obtained as $L_{\text{tot}}^{\text{c}} = 11$ nm, when the total system energy $E_{\text{tot}} = 0$. This is in good agreement with MD simulations, as discussed in the following.

Figure 3 shows a stability map for the self-folding of single-layer graphenes obtained from MD simulations. The stability map presents two critical lengths which divide the graphene self-folding into three regimes: (1) for $L_{\text{tot}} < 6.5$ nm, only flat configuration is stable; (2) for 6.5 nm $< L_{\text{tot}} <$ 10.5 nm, the self-folded graphene is metastable, both flat and self-folded configurations could exist, but the self-folded graphene can be unfolded when the temperature increases; (3) for $L_{\text{tot}} > 10.5$ nm, the self-folded configuration is more stable than the flat graphene, which implies that a flat graphene with length larger than 10.5 nm would self-fold to form a bilayer edge.

We have also compared our finite deformation model with previous small deformation models on the prediction of critical folding length. The small deformation model gives the critical folding length to be 11.6 nm, slightly larger than 11 nm predicted by our study. To illustrate this difference under different conditions, various adhesion energies in the range 0.14–2.8 eV nm^{-2}, corresponding to 1/10 to 2 times of $\gamma = 1.45\,\text{eV nm}^{-2}$ between graphene layers, were adopted. Critical folding length of graphene with varying adhesion energies is shown in figure 3(*b*). It is shown that the small deformation model always gives slightly larger critical folding length than our finite deformation model.

The profile of a folded graphene is very important for predicting the electronic properties of the bilayer edge. The x and y coordinates given by equation (14) are plotted in figure 4(*a*), demonstrating the profile of a folded single-layer graphene. The folded edge clearly shows a racket shape. Since the optimal half-length of the folded region L is always 2.5 nm, as shown in figure 2, the racket shape does not change with the total length of the graphene. This is also verified by MD simulations. The profile obtained by MD simulation is also presented in figure 4(*a*), which shows good agreement with the analytical solution. For comparison, the profile predicted by small deformation theory is also presented in figure 4(*a*), which shows a sharp, discontinuous point at the right end. This is because approximate expression of slope $\theta = \text{d}y/\text{d}x$ rather than $\sin\theta = \text{d}y/\text{d}s$ is usually used in previous small deformation models. Clearly, small deformation theory gives the profile of folded graphene edge remarkably different from those obtained by MD simulations and large deformation theory, and hence cannot be used to predict the profile of folded graphene edges.

MD simulations are also used to study the effect of folding directions on the profile of the folded graphene edges. As shown in figure 4(*b*), the edge profiles by folding a single-layer graphene along different directions exhibit almost identical shapes. This indicates negligible influence of folding directions on the shape of folded graphene edge.

5. Conclusions

A theoretical model based on finite deformation beam theory has been established to predict the self-folding of single-layer graphene. Critical graphene lengths for metastable and stable folding are given. The profile of the folded graphene can

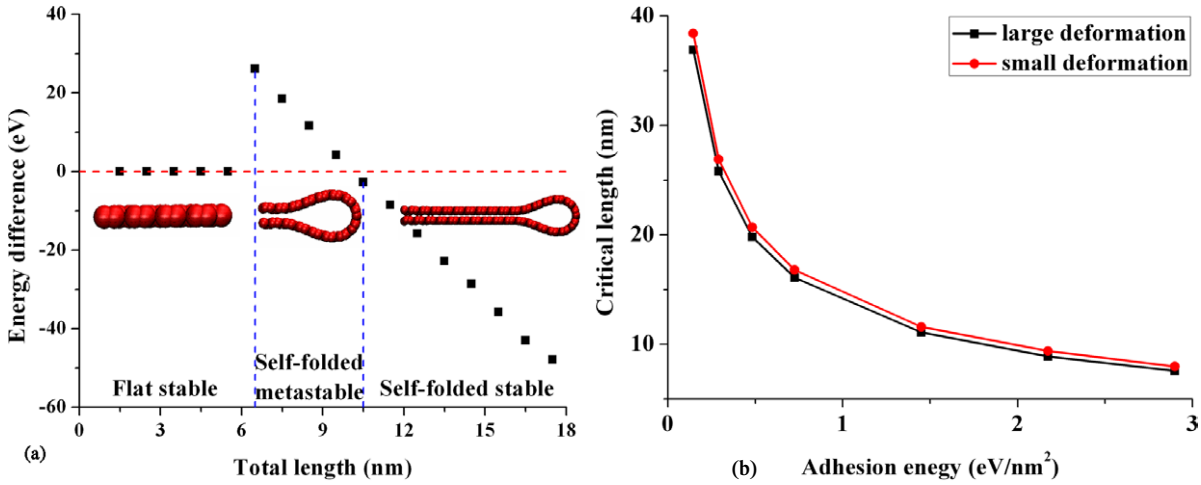

Figure 3. (*a*) Stability map of self-folding of single-layer graphenes, (*b*) comparison of critical folding length between finite deformation and small deformation models, for different adhesion energies.

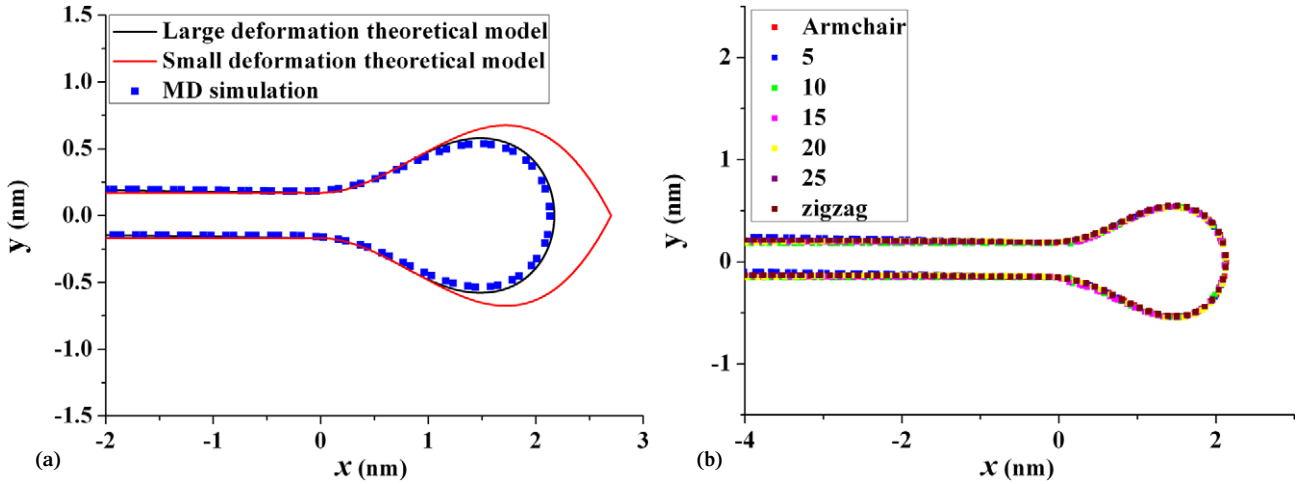

Figure 4. (*a*) Profile of a folded single-layer graphene predicted by MD simulations, and finite and small deformation models; (*b*) influence of folding directions on the profile of folded single-layer graphenes.

also be accurately predicted. MD simulations are performed, which show good agreement with theoretical results. It is also shown that the folding direction does not exhibit strong influence on the shape of folded graphene edges. The results can have important implications for the design and fabrication of graphene nanoelectronics and devices.

Acknowledgments

The financial support by the Natural Science Foundation of China (Grant 11172022) and the Major Project of Chinese National Programs for Fundamental Research and Development 2010CB832703 are gratefully acknowledged. ML acknowledges the startup support from the Fundamental Research Funds for the Central Universities. JX also acknowledges the startup support from the College of Engineering and Applied Science of University of Colorado Boulder.

References

[1] Bunch J S, van der Zande A M, Verbridge S S, Frank I W, Tanenbaum D M, Parpia J M, Craighead H G and McEuen P L 2007 *Science* **315** 490–3
[2] Meyer J C, Geim A K, Katsnelson M I, Novoselov K S, Booth T J and Roth S 2007 *Nature* **446** 60–3
[3] Castro Neto A H, Guinea F, Peres N M R, Novoselov K S and Geim A K 2009 *Rev. Mod. Phys.* **81** 109–62
[4] Lee C, Wei X, Kysar J W and Hone J 2008 *Science* **321** 385–8
[5] Geim A K and Novoselov K S 2007 *Nature Mater.* **6** 183–91
[6] Zhu Y, Murali S, Cai W, Li X, Suk J W, Potts J R and Ruoff R S 2007 *Adv. Mater.* **22** 3906–24
[7] Li X *et al* 2009 *Science* **324** 1312–4
[8] Zhu Y *et al* 2011 *Science* **332** 1537–41
[9] Bunch J S, Verbridge S S, Alden J S, van der Zande A M, Parpia J M, Craighead H G and McEuen P L 2008 *Nano Lett.* **8** 2458–62
[10] Koenig S P, Boddeti N G, Dunn M L and Bunch J S 2011 *Nature Nano* **6** 543–6
[11] Koenig S P, Wang L, Pellegrino J and Bunch J S 2012 *Nature Nano* **7** 728–32

[12] Weiss N O, Zhou H, Liao L, Liu Y, Jiang S, Huang Y and Duan X 2012 *Adv. Mater.* **24** 5782–5
[13] Novoselov K S, Falko V I, Colombo L, Gellert P R, Schwab M G and Kim K 2012 *Nature* **490** 192–200
[14] Zhang J, Xiao J, Meng X, Monroe C, Huang Y and Zuo J-M 2010 *Phys. Rev. Lett.* **104** 166805
[15] Feng J, Qi L, Huang J Y and Li J 2009 *Phys. Rev.* B **80** 165407
[16] Liu Z, Suenaga K, Harris P J F and Iijima S 2009 *Phys. Rev. Lett.* **102** 015501
[17] Son Y-W, Cohen M L and Louie S G 2006 *Phys. Rev. Lett.* **97** 216803
[18] Nakada K, Fujita M, Dresselhaus G and Dresselhaus M S 1996 *Phys. Rev.* B **54** 17954–61
[19] Enoki T, Kobayashi Y and Fukui K-I 2007 *Int. Rev. Phys. Chem.* **26** 609–45
[20] Ritter K A and Lyding J W 2009 *Nature Mater* **8** 235–42
[21] Zhan D, Liu L, Xu Y N, Ni Z H, Yan J X, Zhao C and Shen Z X 2011 *Sci. Rep.* **1** 12
[22] Warner J H, Rummeli M H, Bachmatiuk A and Buchner B 2010 *Nanotechnology* **21** 325702
[23] Zhou W, Huang Y, Liu B, Hwang K C, Zuo J M, Buehler M J and Gao H 2007 *Appl. Phys. Lett.* **90** 073107
[24] Buehler M J, Kong Y, Gao H J and Huang Y G 2006 *J. Eng. Mater. Technol.—Trans. ASME* **128** 3
[25] Xiao J L, Liu B, Huang Y, Hwang K C and Yu M F 2007 Stability and charality effect on twist formation of collapsed double wall carbon nanotubes *Trans. Nonferrous Met. Soc. China* **16** S776–9
[26] Xiao J, Liu B, Huang Y, Zuo J, Hwang K C and Yu M F 2007 *Nanotechnology* **18** 395703
[27] Cranford S, Sen D and Buehler M J 2009 *Appl. Phys. Lett.* **95** 123121
[28] Tarsicio B, Cristian N and Augusto B 2002 *Eur. J. Phys.* **23** 371
[29] Plimpton S 1995 *J. Comput. Phys.* **117** 1–19
[30] Humphrey W, Dalke A and K Schulten 1996 *J. Mol. Graphics* **14** 33–8
[31] Stuart S J, Tutein A B and Harrison J A 2000 *J. Chem. Phys.* **112** 6472–86
[32] Brenner D W, Shenderova O A, Harrison J A, Stuart S J, Ni B and Sinnott S B 2002 *J. Phys.: Condens. Matter* **14** 783–802
[33] Huang Y, Wu J and Hwang K C 2006 *Phys. Rev.* B **74** 245413
[34] Liu B, Yu M-F and Huang Y 2004 *Phys. Rev* B **70** 161402
[35] Girifalco L A, Hodak M and Lee R S 2000 *Phys. Rev.* B **62** 13104–10
[36] Zhu L, Wang Z, Wang Y, Zou G, Mao H and Ma Y 2011 *Phys. Rev. Lett.* **106** 255503
[37] Kudin K N and Scuseria G E 2001 *Phys. Rev.* B **64** 235406